RESEARCH ARTICLE | MAY 23 2017

Compact, high-repetition-rate source for broadband sum-frequency generation spectroscopy

Zsuzsanna Heiner ; Valentin Petrov; Mark Mero

APL Photonics 2, 066102 (2017)
https://doi.org/10.1063/1.4983691

Compact, high-repetition-rate source for broadband sum-frequency generation spectroscopy

Zsuzsanna Heiner,[1,2,a] Valentin Petrov,[3] and Mark Mero[3]
[1]*School of Analytical Sciences Adlershof SALSA, Humboldt-Universität zu Berlin, Berlin 12489, Germany*
[2]*Department of Chemistry, Humboldt-Universität zu Berlin, Berlin 12489, Germany*
[3]*Max Born Institute for Nonlinear Optics and Short Pulse Spectroscopy, Berlin 12489, Germany*

(Received 5 March 2017; accepted 4 May 2017; published online 23 May 2017)

We present a high-efficiency optical parametric source for broadband vibrational sum-frequency generation (BB-VSFG) for the chemically important mid-infrared spectral range at 2800–3600 cm^{-1} to study hydrogen bonding interactions affecting the structural organization of biomolecules at water interfaces. The source consists of a supercontinuum-seeded, dual-beam optical parametric amplifier with two broadband infrared output beams and a chirped sum-frequency mixing stage providing narrowband visible pulses with adjustable bandwidth. Utilizing a pulse energy of only 60 μJ from a turn-key, 1.03-μm pump laser operating at a repetition rate of 100 kHz, the source delivers 6-cycle infrared pulses at 1.5 and 3.2 μm with pulse energies of 4.6 and 1.8 μJ, respectively, and narrowband pulses at 0.515 μm with a pulse energy of 5.0 μJ. The 3.2-μm pulses are passively carrier envelope phase stabilized with fluctuations at the 180-mrad level over a 10-s time period. The 1.5-μm beamline can be exploited to deliver pump pulses for time-resolved studies after suitable frequency up-conversion. The high efficiency, stability, and two orders of magnitude higher repetition rate of the source compared to typically employed systems offer great potential for providing a boost in sensitivity in BB-VSFG experiments at a reduced cost. [http://dx.doi.org/10.1063/1.4983691]

I. INTRODUCTION

Vibrational sum-frequency generation (VSFG) spectroscopy is a powerful tool to study the structure, orientation, and dynamics at surfaces and buried interfaces between two centrosymmetric or random-phase media at the molecular level.[1] In a typical VSFG setup, a non-resonant, narrow-bandwidth (i.e., picosecond) visible (VIS) pulse mixes with a narrow-bandwidth infrared (IR) pulse that is resonant with a vibrational transition of the interfacial molecules. The advent of tunable femtosecond pulses led to the development of broadband VSFG spectroscopy, where single-shot acquisition of spectra for whole vibrational regions became possible without laboriously scanning the wavelength of a narrowband infrared source.[2] Broadband VSFG (BB-VSFG) spectroscopy has also provided an opportunity for ultrafast surface dynamic studies and the higher stability, repetition rate, and peak intensity of such laser pulses significantly improved the signal-to-noise ratio.[3] However, even though VSFG spectroscopy reached sub-monolayer sensitivity, a further two–three order of magnitude improvement in sensitivity is required to be able to study certain important molecules at small surface coverages.[4]

Standard BB-VSFG spectroscopy setups rely on Ti:sapphire pump lasers.[2,3,5] In these setups, 100's of μJ of pump pulse energy is utilized at kHz repetition rates both for producing the broadband IR and the narrowband VIS pulses at the few-μJ-level corresponding to average powers of a few mW.

[a]heinerzs@hu-berlin.de

The IR pulses are obtained from difference-frequency mixing and/or optical parametric amplification (OPA). The production of synchronized narrowband VIS pulses typically relies on convenient, but highly inefficient spectral filtering of the femtosecond pump pulses based on bandpass filters and zero-dispersion monochromators.[3] Electronic synchronization of a spectrally narrowband ps laser amplifier to a fs amplifier is also possible, but cumbersome.[6] Spectral filtering using low-throughput etalons[7] and efficient second-harmonic generation (SHG) in long nonlinear crystals[8] are less widespread, but are able to suppress the nonresonant SFG background from the sample by creating temporally asymmetric, narrowband pulses. The low efficiency in the typically employed VIS pulse generation schemes and the significant quantum defect of Ti:sapphire laser amplifiers limit the scalability of BB-VSFG spectroscopy to high repetition rates.

On the other hand, diode-pumped ps and sub-ps Nd-/Yb-laser systems are gaining wide popularity due to their lower cost, higher robustness, and greater average power scalability compared to the more traditional Ti:sapphire pump lasers. Recently, several high repetition rate (i.e., $\gg$10 kHz) OPA sources driven by such pump systems have been demonstrated in the mid-IR (MIR) and particularly in the spectral range around 3 μm.[9–16] The short, $\leq$1 ps pump pulses provided by Yb lasers allow supercontinuum seed pulse generation and simple dispersion management for the OPA.[9,14–16]

Here, we present a small-scale, high-efficiency BB-VSFG system driven by only 60 μJ (i.e., 6 W at 100 kHz) from a compact, commercial ultrafast Yb pump laser. The system has been developed to study organic molecules with the fundamental stretching modes of their O–H, N–H, and C–H bonds lying in the 2.7–3.6-μm (i.e., 2800–3600 cm^{-1}) spectral region. It consists of three optically synchronized outputs: at ~3.2, ~1.5, and 0.515 μm, with pulse energies and pulse durations of 1.8, 4.6, and 5.0 μJ and 60 fs, 30 fs, and 4.5 ps, respectively. The narrowband VIS pulses are produced using a sum-frequency generation scheme allowing small, adjustable spectral bandwidths at high conversion efficiency.[17] The two IR beams are obtained from a supercontinuum-seeded dual-beam OPA, where the seed pulses in each OPA stage are centered at ~1.5 μm, and the MIR pulses are extracted only at the last stage. This design provides more straightforward construction and optimization of the OPA system due to the availability of off-the-shelf optical components and sensors in the pump and seed spectral range in contrast to the MIR. In addition, the higher pulse energies at the 1.5-μm output, when the OPA is seeded at 1.5 μm, can be exploited using frequency up-conversion for generating pump pulses with sufficiently high energies for time-resolved experiments.

II. EXPERIMENTAL SETUP AND RESULTS

The scheme of the OPA system is shown in Fig. 1. It is driven by a single, compact, turn-key 1.03-μm Yb:KGd(WO$_4$)$_2$ laser oscillator-amplifier system (Pharos-SP, Light Conversion Ltd.) operated at a repetition rate of 100 kHz with a pulse duration of 180 fs, which is comparable to that of

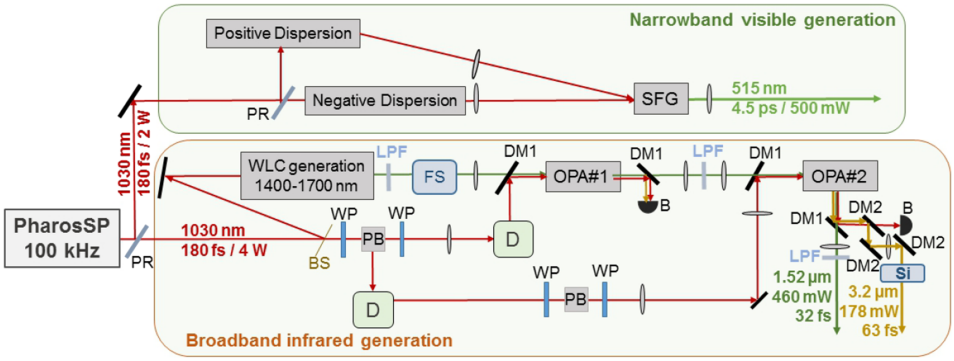

FIG. 1. Schematic layout of the triple-beam setup for the generation of narrowband VIS and broadband IR pulses. BS: beam sampler, PR: partial reflector, WP: half-wave plate, PB: Brewster-type thin film polarizing beam splitter, D: delay stage, FS: fused silica window, Si: silicon window, LPF: long-pass filter, B: beam dump. DM1: dichroic mirror, highly reflective (HR) at 1.03 μm/2.6–3.6 μm, highly transmitting (HT) at 1.4–1.7 μm, DM2: dichroic mirror, HR at 2.7–3.6 μm, HT at 1.03 μm/1.3–1.7 μm. All lenses, wave plates, crystals, and filters are AR-coated.

typical Ti:sapphire regenerative amplifiers. Out of the total pulse energy of 60 μJ available from the pump laser, only 40 μJ is used for pumping and seeding the OPA, while the remaining 20 μJ is used for generating the narrowband VIS pulses.

A. Generation of broadband, dual-beam infrared pulses

The seed pulses of the present source are supercontinuum pulses generated by the femtosecond pump pulses, providing robust optical synchronization between the pump and signal/idler waves from the OPA. As in Ref. 14, (i) the OPA is seeded by the continuum on the Stokes side of the Yb pump and (ii) is based on periodically poled lithium niobate (PPLN), enabling a simplified, high gain setup. Compared to Ref. 14, the fan-out type crystals, a longer crystal in the booster amplifier, and the much lower pump average powers/peak intensities in our case allowed significantly higher overall conversion efficiency in fewer OPA stages while still preserving few-cycle compressed pulse durations, high beam quality, and high long term stability in both IR beamlines. In contrast to our work, the OPA systems in Refs. 15 and 16 are both large-scale, single-beam sources optimized for the MIR (i.e., employing MIR seed pulses) in order to maximize their utility for high-harmonic generation, and therefore, the second IR beamline was dumped and not characterized.

For OPA seed generation, a small fraction (i.e., 1.1 μJ) of the total energy (40 μJ) was split off using a beam sampler and focused into a 6-mm thick uncoated YAG window to generate a single-filament continuum. A long-pass filter was used to block the pump beam and transmit the >1.3-μm part of the continuum. As in the case in Refs. 11 and 14, the group-delay dispersion (GDD) in the seed/signal arm was chosen to be positive in order that the idler beam generated in the booster OPA stage exhibits down-chirp, which can be removed by widely available anti-reflection (AR) coated silicon windows in their positive GDD spectral range. The up-chirp arising from the continuum generation process was partly compensated by two AR-coated fused silica (FS) windows with a total thickness of 24 mm. In this way, the 1.4–1.7-μm portion of the continuum was kept within the short pump time window, while still maintaining its up-chirp.

The pre-amplifier (cf. OPA#1 in Fig. 1) is a 1-mm long, AR-coated, 5% MgO-doped, fan-out PPLN crystal with a grating period varying from 21 to 34 μm across the 5.1-mm-wide aperture (HC Photonics Corp.) operated at room temperature in collinear geometry. The continuum seed pulses are focused by an f = 500-mm achromat through a dichroic mirror to a beam waist radius (i.e., w_{1/e^2}) of 200 μm at the crystal. Pumped by 5.1 μJ at a peak intensity of only 45 GW/cm^2, the first stage yields an amplified signal pulse energy of 0.4 μJ, corresponding to a pump-to-signal energy conversion efficiency of 8%. The MIR idler beam generated in this stage and the residual pump beam are filtered out by a dichroic reflector and a long-pass filter.

The booster amplifier (cf. OPA#2 in Fig. 1) is based on a 2-mm long, 2-mm thick PPLN crystal, analogous to OPA#1, operated at 150 °C and also used in collinear geometry. The 28.5-μJ (i.e., 2.85-W average power) incident pump pulses are down-collimated to a beam waist radius of 500 μm at the crystal, leading to a somewhat lower peak intensity of 40 GW/cm^2 than in the pre-amplifier. The gain in OPA#2 is in excess of 10, leading to an output signal pulse energy of 4.6 μJ (i.e., 460-mW average power) as measured after a dichroic mirror, a re-collimating achromat, and a long-pass filter. The pump-to-signal energy conversion efficiency is 15%. We estimated an upper limit for the amplified superfluorescence background in the signal beam by measuring the output power of the fully pumped OPA system with the seed blocked and obtained a negligible value below the nominal 0.2-mW resolution of our power meter head. The MIR idler pulses generated in OPA#2 are separated from the signal and the pump beams by dichroic optics and re-collimated by a CaF_2 singlet lens. The so-obtained idler beam exhibits a pulse energy of 1.8 μJ, corresponding to an average power of 180 mW. The area on the optical table used for the entire OPA source was 0.5 m^2.

The signal and idler pulses were characterized using SHG-frequency resolved optical gating (SHG-FROG). A single multi-shot FROG apparatus with replaceable, AR-coated pellicle beam splitters was used for both beams. For the signal/idler beam, a 0.5-mm thick β-BaB_2O_4 (BBO)/0.2-mm thick $AgGaS_2$ (AGS) type-I crystal was used, respectively. The non-collinear angle between the beams incident on the nonlinear crystal was 2°. The amplified signal pulses were found to be reasonably close to the transform-limited value without adding extra bulk material for dispersion compensation, i.e., the substrates of the transmissive optics after OPA#2 served as the compressor.

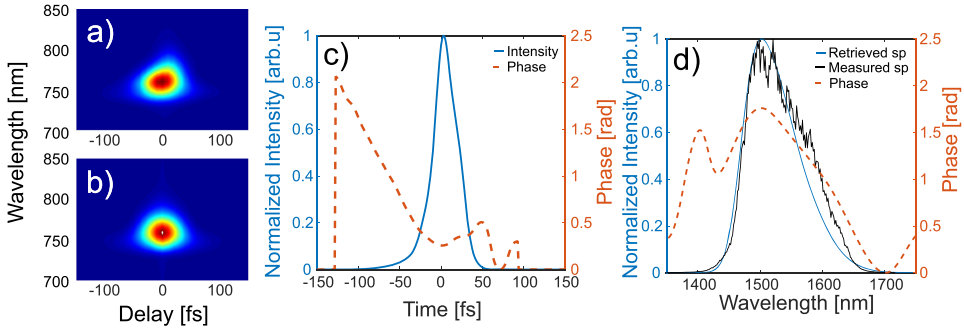

FIG. 2. SHG-FROG characterization of the 4.6-μJ amplified signal pulses: Measured (a) and retrieved (b) SHG-FROG spectrogram, retrieved temporal intensity and phase (c), and spectral intensity (sp) and phase (d). The measured spectrum is also shown in (d). The FROG-error of the reconstruction for a grid size of 64 × 64 points was 0.0099.

The measured and retrieved FROG traces together with the reconstructed temporal and spectral profiles of the amplified signal pulses at the highest power are shown in Fig. 2. The measured pulse duration at FWHM intensity was 32 fs (i.e., 6.3 cycles at 1.52 μm), which is 23% longer than the 26-fs transform-limited value.

The output idler pulse duration was minimized using AR-coated silicon windows, which exhibit positive GDD at 3.2 μm and ~5% loss per window. The optimum window thickness was found to be 5 mm, leading to transform-limited pulse duration at 63-fs FWHM (<6 cycles at 3.2 μm). Figure 3 shows the corresponding FROG data and the measured idler spectrum, which exhibits a spectral full width of ~600 nm (590 cm^{-1}) at a central wavelength of 3.2 μm (3125 cm^{-1}). The spectral windows of the dichroic reflectors DM1 and DM2 (cf. Fig. 1) also allow some minor spectral tunability of the central wavelength of ±200 nm, while still preserving few-cycle pulse durations. The spectral tuning is achieved by varying the pump-seed time delay and the transverse position and tilt angle of the OPA crystals.

The average power stability of the output signal and idler beams was high, in spite of the lack of a beam enclosure during the measurements, as demonstrated in Fig. 4. The very small, monotonous drop in average power is attributed to a drift in lab temperature. In the measured 1.75–2-h time windows, the fluctuations including the slow drift are at the ≤0.4% RMS level. The measured near-field beam profiles are nearly Gaussian and are also shown in Fig. 4.

As the seed and pump pulses in OPA#2 are originating from the same pump laser, the generated idler pulses are predicted to be CEP (carrier-envelop phase) stable.[18] Even though CEP-stability of the laser pulses is currently not crucial in VSFG spectroscopy, other types of spectroscopy can benefit from low CEP noise. In order to characterize the CEP jitter, we employed f–2f interferometry utilizing a single-beam setup.[19] The necessary continuum was produced by focusing the compressed idler pulses using a 50-mm CaF_2 singlet lens into a 2-mm thick uncoated YAG window. A supercontinuum

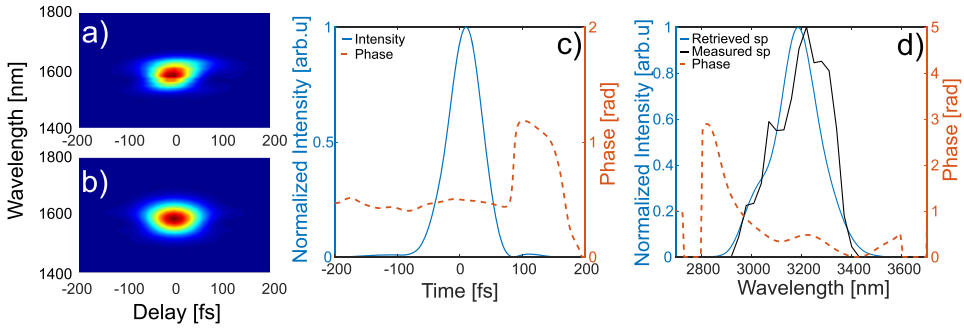

FIG. 3. SHG-FROG characterization of the 1.8-μJ output idler pulses: measured (a) and retrieved (b) SHG-FROG spectrogram, retrieved temporal intensity and phase (c), and spectral intensity (sp) and phase (d). The measured spectrum is also shown in (d). The FROG-error of the reconstruction for a grid size of 64 × 64 points was 0.011.

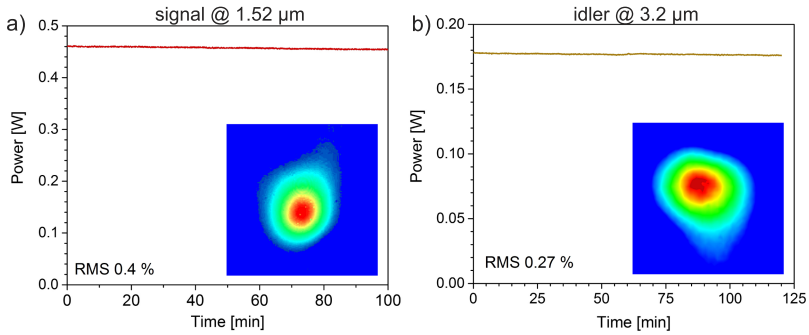

FIG. 4. Average power stability of the 1.52-μm, 32-fs, 4.6-μJ signal pulses (a) and the 3.2-μm, 63-fs, 1.8-μJ idler pulses (b). The sampling rate of the power meter was 10 Hz. The insets show the beam profiles of the collimated output beams with w_{1/e^2} (horizontal) = 2.4/3.6 mm and w_{1/e^2} (vertical) = 3/3.2 mm for the signal/idler, respectively.

stretching down to 450 nm was generated. A similar multi-octave continuum produced by a state-of-the-art 3-μm source and its use for CEP noise characterization were reported in Ref. 20. In our setup, which was following essentially the same scheme as in Fig. 3 of Ref. 20, the continuum was collimated with a 25-mm focal length N-BK7 achromatic lens, which also eliminated the fundamental MIR beam, and was focused into a 1-mm thick type-I BBO crystal. The phase-matching angle was adjusted to frequency-double the wavelength range around 1.3-μm. The emerging second harmonic and the fundamental ~650-nm wave packet in the supercontinuum were relay-imaged with a 100-mm focal length ultraviolet grade fused silica (UVFS) lens onto the slit of a CCD spectrometer. A wire grid polarizer was used to maximize the visibility of the resulting spectral fringes. Figure 5(a) shows the so-obtained fringes as a function of time over a few-second period. The PPLN temperature was 150 °C. In order to show that the fringes proved CEP stability, we inserted a 3-mm thick UVFS window into the collimated MIR continuum [cf. at 10.5 s in Fig. 5(a)] and the resulting change in fringe period was measured. With no window in the beam, the measured fringe period was 4.5 nm at a center wavelength of 650 nm. Based on the Sellmeier equation of fused silica, the expected change in the group delay between the 1.3-μm and 650-nm wave packets will lead to a fringe period of 3.2 nm. This is in excellent agreement with the experimental value of 3.1 nm. Figure 5(b) shows the fringe stability over a period of 10 s characterized by an RMS value of 180 mrad. Heating of OPA#2 improved the long-term CEP stability. Figures 5(c) and 5(d) show CEP fringes recorded over a 5-min period at 150 °C and at room temperature, leading to RMS fluctuations of 320 and 890 mrad, respectively. We attribute the improved CEP stability at a higher PPLN crystal temperature to suppressed photorefractive effects known to occur even in MgO-doped PPLN.[21] We note that higher PPLN temperatures did not lead to higher OPA efficiency.

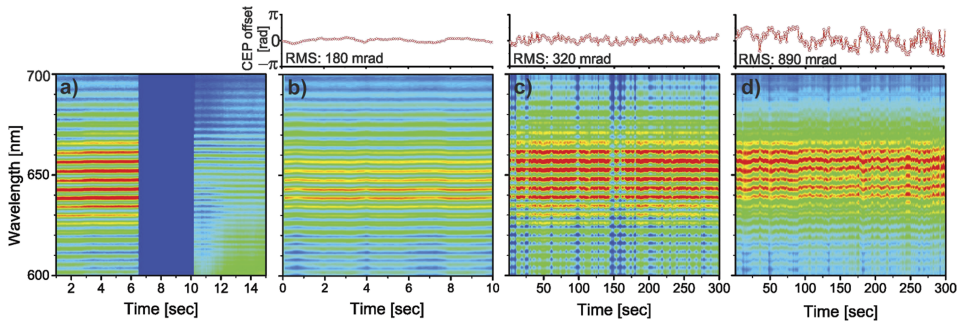

FIG. 5. CEP spectral interference fringes as a function of time obtained using an f–2f interferometer over various time periods and PPLN crystal temperature in OPA#2. (a) A 3-mm thick UVFS plate was inserted in the supercontinuum prior to SHG at 10.5 s. The beam was blocked by the mount of the UVFS window between 7 and 10.5 s. (b) 180-mrad RMS jitter over a 10-s period at a PPLN temperature of 150 °C. (c) 320-mrad RMS jitter over a 5-min period at a PPLN temperature of 150 °C. (d) 890-mrad RMS jitter over a 5-min period at a PPLN temperature of 22 °C. The sampling rate/integration time of the spectrometer were 10 Hz/30 ms [(a) and (b)] and 1 Hz/30 ms [(c) and (d)], respectively.

B. Generation of narrowband visible pulses

The typical spectral resolution in BB-VSFG is a few 1 cm^{-1} dictated by the bandwidth of the VIS pulse. The high losses of the spectral filtering scheme usually used for producing the narrowband VIS pulses lead to an expensive setup. Employing an efficient SFG-spectral compression technique,[17] we achieved an overall conversion efficiency of 25% making it possible to use the low-energy, compact pump laser in a cost-effective way. The 20-μJ, 1.03-μm pulses are split into two beams with equal power and are sent into a positive (folded Martinez stretcher) and a negative (folded Treacy compressor) dispersion unit. Each dispersion unit employed free-space transmission gratings with a groove density of 1000 l/mm, where GDD with equal magnitude but opposite sign is imposed on the pulses stretching them to a duration of 6.8 ps in both arms. After chirped SFG in a 1.5-mm-thick, type-I BBO crystal, 5.0-μJ, 4.5-ps pulses are obtained with excellent beam quality. The spectrum of the visible pulses is shown in Fig. 6(a), where the instrument resolution limited the spectral bandwidth to ~4.9 cm^{-1}. Assuming transform-limited 4.5-ps Gaussian visible pulses, a spectral FWHM of ~3.0 cm^{-1} is obtained through Fourier transformation. The spectral bandwidth of the VIS pulses is tunable and can also be reduced below 1 cm^{-1} by increasing the GDD in the dispersion units and re-optimizing the focusing conditions to keep the conversion efficiency constant in the chirped SFG step. The center wavelength of the narrowband pulses is also slightly tunable in the 515 ± 4-nm-range by changing the time delay between the positive and negative GDD arms. The area on the optical table used for the VIS pulse generation unit was 0.3 m^2.

C. Generation of sum-frequency signal on a gold surface

In order to demonstrate that the source can be used to obtain broadband surface SFG spectra with good signal-to-noise ratio at short integration times, we acquired the SFG signal from a Au(111) surface, which is a typical preparatory step used for optimizing the temporal and spatial overlap of the IR and VIS pulses prior to studying a real sample. The MIR and VIS pulses were focused on the sample using an $f = 50$-mm and an $f = 300$-mm singlet lens at angles of incidence of 52° and 62°, respectively. The generated sum-frequency signal was detected using a 320-mm spectrograph equipped with a Peltier-cooled, deep-depletion CCD. Figures 6(b) and 6(c) show the primary BB-VSFG data sets, the spectrally resolved intensity cross correlation signal and the sum-frequency spectrum at zero-delay (i.e., taken from the cross correlation trace), respectively, generated by the broadband MIR and the narrowband VIS pulses at the air-gold interface. Due to the very short MIR pulse compared to the visible pulse, the intensity cross correlation function is proportional to the temporal shape of the visible pulse with a FWHM of ~4.5 ps. As the 0.515-μm pulses are narrowband, the spectrum shown in Fig. 6(c) also allows an independent measurement of the spectrum of the 3.2-μm pulses. We note that the signal generated at a gold surface is a more reliable representation of the actual MIR spectrum than either (i) the spectrum measured by the PbSe spectrometer showing signs of a nonlinear response or (ii) the FROG-reconstructed spectrum relying on an InGaAs spectrometer, which was limited to wavelengths below 1.7 μm (i.e., the second-harmonic of MIR wavelengths above 3.4 μm could not be detected). The infrared frequency axis extracted from the SFG spectrum was calibrated by measuring the absorption spectrum of polystyrene using the nonresonant SFG signal from the gold surface. The SFG spectrum obtained at the gold surface is featureless, but when a biaxially oriented, 50-μm-thick

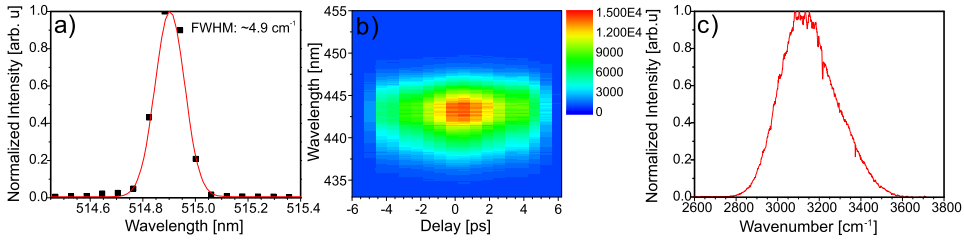

FIG. 6. (a) Spectrum of the narrowband visible pulses with a FWHM ~4.9 cm^{-1} limited by the spectrograph-CCD system. (b) Spectrally resolved intensity cross correlation signal and (c) sum-frequency spectrum at zero-delay taken from (b), obtained by mixing the broadband 3.2-μm and the narrowband 0.515-μm pulses at an uncoated gold surface in the $P_{SFG}P_{VIS}P_{MIR}$ polarization state. In (b) and (c), the grating line density was 2400 1/mm and an integration time of 1 s was used.

polystyrene film is inserted into the MIR beam path, it shows sharp attenuation at the MIR absorption bands of polystyrene. The absorption band of polystyrene at 2850 cm^{-1} (i.e., 3.51 μm) was detected with a high signal-to-noise ratio confirming that the spectrum of the MIR beam extended beyond the cutoff wavelengths of the spectra in Fig. 3(d).

III. CONCLUSIONS

We have presented a triple-beam, high-repetition-rate BB-VSFG source pumped by a 1.03-μm, low-cost, turn-key laser, providing both narrowband pulses at 0.515 μm and broadband and few-cycle pulses at 1.52 and 3.2 μm; all optically synchronized and exhibiting excellent long-term stability. The two orders of magnitude higher repetition rate compared to typical BB-VSFG setups and the high stability are expected to lead to a significantly improved signal-to-noise ratio in VSFG spectroscopic applications. Thanks to the fan-out type PPLN crystals used for generating the broadband pulses, the large amplification bandwidth in the IR could be preserved at high conversion efficiencies in a very compact and simple setup. The narrowband VIS pulse generation scheme employed also offers a potentially sub-1-cm^{-1} resolution in VSFG experiments. In spite of the limited pump pulse energy, IR and VIS average powers at the level of 100's of mW were obtained, sufficient to drive a wide range of nonlinear spectroscopic applications. Both IR beams could be compressed to near their 5–6-cycle transform limit using only bulk materials. The CEP-stable, 3.2-μm pulses exhibit a spectral full width of ~800 cm^{-1}, thereby covering a large portion of the spectroscopically important MIR spectral range around 3 μm. The additional IR beamline at 1.5 μm can be used for ultrafast surface dynamic studies after a suitable frequency up-conversion step.

ACKNOWLEDGMENTS

We thank Janina Kneipp for the support and helpful suggestions. Funding by the Deutsche Forschungsgemeinschaft (DFG), No. GSC 1013 SALSA and Leibniz-Gemeinschaft Grant No. SAW-2012-MBI-2 are gratefully acknowledged. Z.H. acknowledges funding by a Julia Lermontova Fellowship from DFG, No. GSC 1013 SALSA.

[1] J. H. Hunt, P. Guyot-Sionnest, and Y. R. Shen, Chem. Phys. Lett. **133**, 189 (1987).
[2] L. J. Richter, T. P. Petralli-Mallow, and J. C. Stephenson, Opt. Lett. **23**, 1594 (1998).
[3] C. S. Tian and Y. R. Shen, Surf. Sci. Rep. **69**, 105 (2014).
[4] H.-F. Wang, L. Velarde, W. Gan, and L. Fu, Annu. Rev. Phys. Chem. **66**, 189 (2015).
[5] E. L. Hommel and H. C. Allen, Anal. Sci. **17**, 137 (2001).
[6] L. Chen, S. Wen, Y. Wang, C. Zhao, L. Qian, and D. Fan, IEEE J. Quantum Electron. **46**, 1354 (2010).
[7] A. Lagutchev, S. A. Hambir, and D. D. Dlott, J. Phys. Chem. C **111**, 13645 (2007).
[8] C. Weeraman, S. A. Mitchell, R. Lausten, L. J. Johnston, and A. Stolow, Opt. Express **18**, 11483 (2010).
[9] M. Bradler, C. Homann, and E. Riedle, Opt. Lett. **36**, 4212 (2011).
[10] B. W. Mayer, C. R. Phillips, L. Gallmann, and U. Keller, Opt. Express **22**, 20798 (2014).
[11] M. Mero, F. Noack, V. Petrov, and M. J. J. Vrakking, Opt. Express **23**, 33157 (2015); M. Mero and V. Petrov, IEEE Photon. J **9**, 3200408 (2017).
[12] M. Baudisch, B. Wolter, M. Pullen, M. Hemmer, and J. Biegert, Opt. Lett. **41**, 3583 (2016).
[13] B. M. Luther, K. M. Tracy, M. Gerrity, S. Brown, and A. T. Krummel, Opt. Express **24**, 4117 (2016).
[14] P. Rigaud, A. V. de Walle, M. Hanna, N. Forget, F. Guichard, Y. Zaouter, K. Guesmi, F. Druon, and P. Georges, Opt. Express **24**, 26494 (2016).
[15] N. Thiré, R. Maksimenka, B. Kiss, C. Ferchaud, P. Bizouard, E. Cormier, K. Osvay, and N. Forget, Opt. Express **25**, 1505 (2017).
[16] G. M. Archipovaite, S. Petit, J.-C. Delagnes, and E. Cormier, Opt. Lett. **42**, 891 (2017).
[17] M. Nejbauer and C. Radzewicz, Opt. Express **20**, 2136 (2012).
[18] A. Baltuska, T. Fuji, and T. Kobayashi, Phys. Rev. Lett. **88**, 133901 (2002).
[19] M. Kakehata, H. Takada, Y. Kobayashi, K. Torizuka, Y. Fujihira, T. Homma, and H. Takahashi, Opt. Lett. **26**, 1436 (2001).
[20] F. Silva, D. R. Austin, A. Thai, M. Baudisch, M. Hemmer, D. Faccio, A. Couairon, and J. Biegert, Nat. Commun. **3**, 807 (2012).
[21] J. R. Schwesyg, M. Falk, C. R. Phillips, D. H. Jundt, K. Buse, and M. M. Fejer, J. Opt. Soc. Am. B **28**, 1973 (2011).